Microchimica Acta (2019) 186: 753
https://doi.org/10.1007/s00604-019-3885-8

ORIGINAL PAPER

Preparation of deep eutectic solvent-based hexagonal boron nitride-molecularly imprinted polymer nanoparticles for solid phase extraction of flavonoids

Xiaoxia Li[1] · Kyung Ho Row[1]

Received: 30 May 2019 / Accepted: 30 September 2019 / Published online: 8 November 2019

Abstract

Hexagonal boron nitride (h-BN) is introduced as a 2D scaffold during the preparation of molecularly imprinted polymers (MIPs). The MIPs were prepared from deep eutectic solvents (DES) or from DES containing h-BN, crosslinking agent (ethylene glycoldimethacrylate), initiator (AIBN), porogen (methanol), and template (quercetin). The recognition site of the monomer is protected by the hydrogen bond of the DES before the MIP is polymerized. The formation of the final MIP was analyzed theoretically using density-functional theory. The nanoparticles were characterized by scanning electron microscopy, nitrogen sorption analysis, thermogravimetry and Fourier transform infrared spectroscopy. The introduction of h-BN resulted in an increase in the surface area of the nanoparticles. They were applied as a solid phase extraction sorbent for the extraction of flavonoids (specifically of quercetin, isorhamnetin and kaempferol) from *Ginkgo biloba* leaves. Following extraction with ethanol, they were quantified by HPLC. The new sorbent has distinctly improved recognition capability for flavonoids compared to conventional MIP nanoparticles.

Keywords Two-dimensional · Scaffold · Ternary DES · Caffeic acid · Monomer · Hydrogen bond · Recognition site · Selective recognition · *Ginkgo biloba* leaves · Density-functional theory

Introduction

Since Southern molecular imprinting technology in 1975, there have been great advances in recent decades [1–3]. This technology has been applied extensively to the recognition and purification of target molecules in a range of research areas. A MIP is a tailor-made recognition material with cavities that can recognize a template molecule selectively [4–6]. In addition, MIPs prepared using traditional techniques have some weaknesses, such as low-affinity binding, low-rate mass transfer, and high diffusion barrier [7–10]. To improve the molecular recognition efficiency of MIPs, many researchers have made many improvements to the synthesis of MIPs, such as the functional monomer, synthetic environment, and polymer structure [11–13].

In the polymerization of MIPs, the polymer usually agglomerates. The agglomerated structure has a low surface area that limits accessibility to the target molecule [12]. H-BN, also known as "white graphene", has a dominant surface-to-volume ratio and representative layered structure similar to graphite. Within a two-dimensional (2D) layer, alternating B and N atoms are linked with each other by strong B-N covalent bonds; the 2D layers are held together by weak van der Waals forces. The larger surface area and polarity of the B-N bonds provide excellent adsorption properties for a variety of samples [14, 15]. Its excellent thermal stability and chemical inertness also allows feasible reclamation potential [16, 17]. Therefore, h-BN can be a perfect adsorbent material.

Deep eutectic solvents (DESs) have attracted wide and crucial interest for the preparation of a range of materials [18–21]. As the optimal substitute for ionic liquids (ILs), DESs have similarity to ILs, such as low-melting-point, low vapor pressure, high conductivity, and excellent solubility for most

Electronic supplementary material The online version of this article (https://doi.org/10.1007/s00604-019-3885-8) contains supplementary material, which is available to authorized users.

✉ Kyung Ho Row
rowkho@inha.ac.kr

[1] Department of Chemistry and Chemical Engineering, Inha University, Incheon 402-751, South Korea

substances. In addition, DESs have some superiority compared to ILs, such as low cost, biodegradability, low toxicity, and better designability. DESs are shaped with a hydrogen bond donor (HBD) and hydrogen bonding acceptor (HBA) via an intermolecular hydrogen bond. Based on the high viscosity and abundant hydrogen bond in DESs, solid particles have advantageous dispersibility that are beneficial for polymerization [22]. Since 2015, DESs have been used in the synthesis of MIPs, and they improved the affinity and selectivity of MIPs significantly [19]. In 2016, Liu et al. applied DESs as a novel functional monomer in the polymerization of MIPs [11].

Density functional theory (DFT) is a computational quantum mechanical modeling method for chemistry, physics, and materials science, which can provide accurate simulations and computations of various intra- or intermolecular interactions to reinforce the experimental conclusions using lower cost methods [23, 24]. DFT calculations have been applied successfully to study the physical and chemical properties of various materials and molecular imprinting technology to validate and optimize technological plans [25].

In previous studies, DES based MIPs exhibit excellent selectivity and bright development prospect. Nevertheless, the reaction mechanism of DESs in polymerization is unclear, which is not conducive to the optimization of chemical process. Therefore, exploration of reaction mechanism of DES in chemical process is very important for development prospect of DES. DESs are expected to have an increasing number of applications in material science based on their special properties [19]. According to previous research, DES and h-BN were used as an eco-friendly functional monomer and 2D scaffold material in polymerization. [9, 10] More than that, the synthetic mechanism of DES and h-BN-MIPs was verified using DFT methods. A ternary DES was modified on the surface of the 2D material. Application of sorbents to flavonoids is of interest as they are widely found widely as secondary metabolites in plants [26, 27]. *Ginkgo biloba* leaves were rich of flavonoid, it can treatment of memory problems, blood disorders and enhancement of cardiovascular function. A type of flavonoid (quercetin, isorhamnetin, and kaempferol) was applied as the target molecules in this study. A novel h-BN-MIP was synthesized and applied as a solid-phase extraction (SPE) adsorbing material for the recognition of flavonoids from *Ginkgo biloba* leaves. These materials were characterized by scanning electron microscopy (SEM), elemental analysis (EA), Fourier transform infrared (FT-IR) spectroscopy, thermogravimetric analysis (TGA), and Brunauer-Emmett-Teller (BET) surface area measurements. The recognition efficiency of the nanoparticles was evaluated by high-performance liquid chromatography (HPLC).

Experimental section

Reagents and materials

Ethylene glycol (EG) (>99.0%), ethylene glycoldimethacrylate (EGDMA) (98%), acetonitrile (MeCN) (>99.9%), and metha1-nol (MeOH) (>99.9%) were purchased from Alfa Aesar (Heysham, UK, www.alfa.com). Quercetin (Que) (>99.0%) was obtained from Tokyo Chemical Industry Co. Ltd. (Tokyo, Japan, www.tcichemicals.com). 2,2-Azobisisobutyronitrile (AIBN) (98%), and choline chloride (ChCl) (>98.0%) were purchased from Duksan Pure Chemicals Co., Ltd. (Ansan, Korea, www.duksan.kr). Caffeic acid (CA) (98%), h-BN (99%), kaempferol (Kae) (>98%), and isorhamnetin (Iso) (>95%) were obtained from Sigma-Aldrich (St Quentin Fallavier, France, www.sigmaaldrich.com). Duksan Pure Chemicals Co., Ltd. (Ansan, Korea, www.duksan.kr) provided all other organic solvents (analytical grade) and inorganic reagents (analytical grade). *Ginkgo biloba* leaves (*Ginkgo biloba* tea) were purchased from a supermarket. Distilled water was filtered using a vacuum pump and filter (HA-0.45, Millipore, USA, www.millipore.com) prior to use. All samples were filtered (MFS-25, 0.2 μm TF, Whatman, USA, www.whatman.com) prior to HPLC analysis.

Preparation

Synthesis of DESs

DESs were composed of CA, ChCl, and EG with different molar ratios (Table S1). The mixture was stirred at 80 °C until a clear and homogeneous liquid formed. The DES that showed the lowest viscosity (at room temperature) were selected and used in the forthcoming research.

Polymerization of h-BN-MIP nanoparticles

h-BN (1 g) was activated at 750 °C for 1 h in a muffle furnace. Subsequently, the processed BN (200 mg) was mixed with the selected DES, stirred (5 min) and treated ultrasonically (10 min). The turbid mixture was stirred at 60 °C for 24 h. In the polymerization of h-BN-MIP nanoparticles, DES (on the surface of h-BN) was applied as a functional monomer. In the control group, DES without BN was applied to the polymerization of MIP nanoparticles.

As shown in Fig. 1a and Table S2, the monomers (DES or DES with h-BN) were mixed with a crosslinking agent (EGDMA), initiator (AIBN), porogen (MeOH), and template (Que). The mixture was stirred and treated ultrasonically until the turbid liquid had dispersed. The dissolved O_2 in the mixture was removed using N_2. The processed mixture was polymerized at 60 °C in an oven for 12 h. NIP and h-BN-NIP were prepared based on the preceding

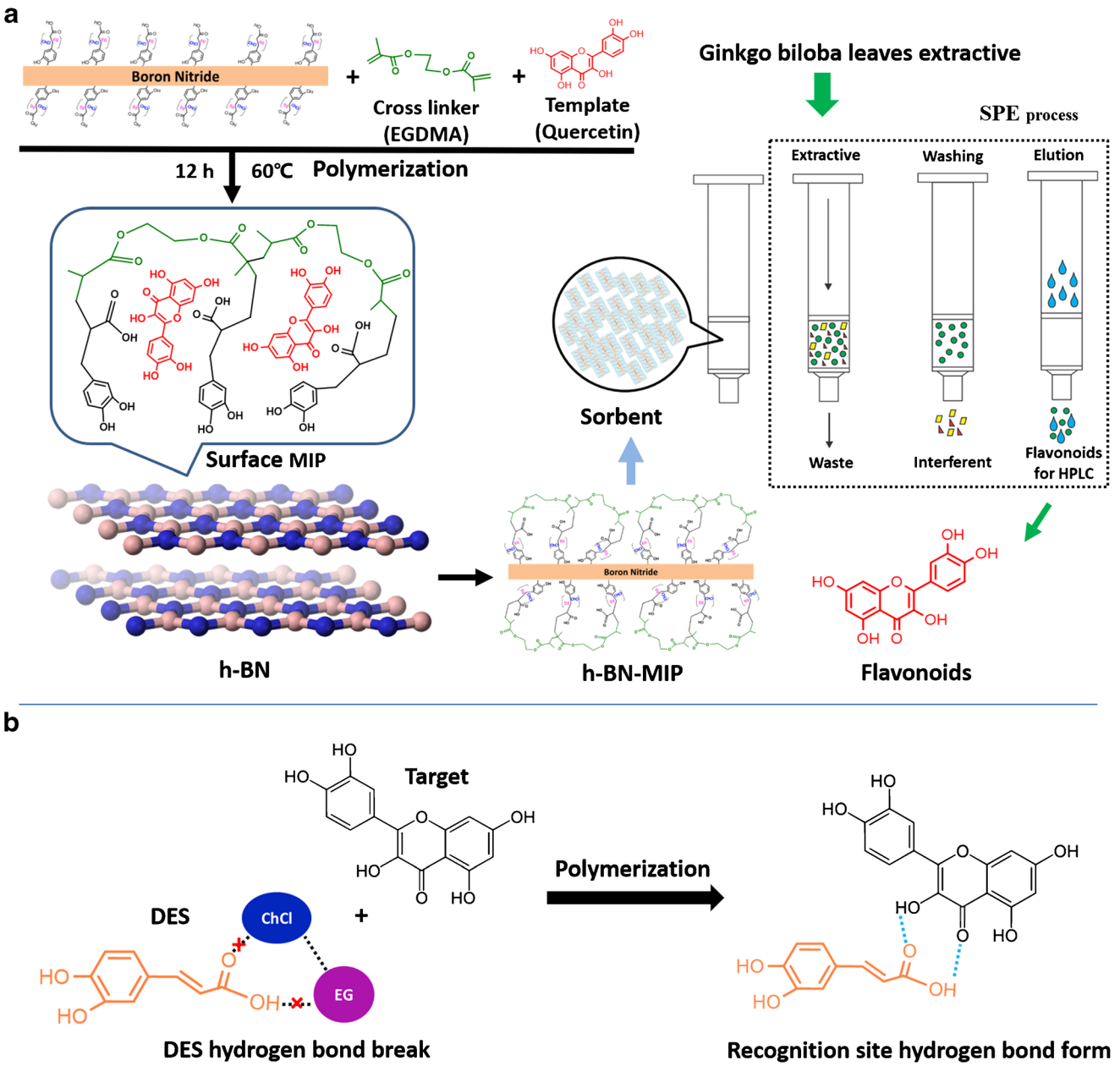

Fig. 1 Schematic diagram of the mechanism for the formation of the h-BN-MIPs and SEP process (**a**). The recognition site of the monomer is protected by the hydrogen bond of the DES before the MIP is polymerized (**b**)

steps without the template. After polymerization, these nanoparticles were washed with methanol in a Soxhlet extractor until the impurities and template were removed completely. After drying and grinding, these nanoparticles were used for the specific recognition of flavonoids.

Theoretical methodology

In a theoretical study, DFT calculations were carried out to optimize the geometry of all the molecules selected in the present study using the Gaussian 09 program (revision D.01) at the B3LYP/6–311 + G(d,p) level of theory. The CA, EG, ChCl, and DES were fully optimized without any symmetry restriction and only the favored conformations are presented. Frequency calculations are essential and were performed on all optimized configurations to confirm that these were the true minima. None of the optimized structures had an imaginary frequency. The thermodynamic properties, such as enthalpy (ΔH), Gibbs free energy (ΔG), and the entropic contribution ($T\Delta S$), regarding the formation process of $(CA)_n$/target complexes ($n = 1$ or 4) were calculated using the following equations:

$$\Delta H = H_{\text{Complexes}} - \left[H_{\text{Target}} + nE_{\text{CA}}\right]$$

$$\Delta G = G_{\text{Complexes}} - \left[G_{\text{Target}} + nG_{\text{CA}}\right]$$

$$T\Delta S = TS_{\text{Complexes}} - \left[TS_{\text{Target}} + nTS_{\text{CA}}\right]$$

Characterization

The C, H, and N contents of the MIPs were examined by elemental analysis (EA1112, Italy). The morphology of the MIPs was observed by SEM (S-4200, Hitachi, Canada). The BET[44] surface area was measured using an ASAP2000 surface area and porosimetry analyzer (Micromeritics, USA). The FT-IR spectra were recorded on a Nicolet iSTO spectrometer (Perkin Elmer, USA) over the wavenumber range of 4000 cm^{-1} to 400 cm^{-1}. TGA (S-1000, Scinco, Korea) was conducted over the range 20 °C to 1000 °C at a heating rate of 10 °C min^{-1} in a nitrogen atmosphere.

Detecting the specific recognition

HPLC conditions

The HPLC-UV system was purchased from Younglin Company (M930, Korea). The analytical column was C_{18} (250 mm × 4.6 mm, 5 μm) column. The mobile phase was MeCN-0.85% H_3PO_4 (95: 5, *v*/v) at 35 °C and its flow rate was set to 1 mL min^{-1}. The wavelength of the UV detector was 370 nm and the injection volume was 10 μL.

Absorption capacity

To assess the level of static adsorption, h-BN-MIP (30 mg) was mixed into the Que. solution (1 mL) and sealed in a miniature centrifuge tube; the concentrations of the Que. solution were 5, 25, 50, 100, 150, 200, 300, and 500 μg mL^{-1}. The mixture was shaken on a shaking table for 12 h at room temperature. In the detection of dynamic adsorption, h-BN-MIP (30 mg) was then mixed into a Que. solution (1 mL, 50 μg mL^{-1}). The mixtures were shaken for 1, 2, 4, 6, 8, 10, and 12 h on a shaking table at room temperature. After absorption, the mixtures were separated by centrifugal separation at 6000 rpm for 15 min. The liquid supernatant was injected into HPLC. h-BN-NIP, MIP, and NIP were operated according to the above steps to determine the absorption capacity.

Validation of re-usability

To validate the re-usability of the 2D-MIP nanoparticles, three levels (5, 25, and 50 μg mL^{-1}) of a quercetin standard solution were used in the adsorption test. A 1 mL aliquot of a standard quercetin solution was added to the SPE column and washed with 1 mL of DI-water. After washing, the target was eluted from the SPE column with 1 mL of ethanol. The eluent collected at a constant volume (1 mL) was analyzed by HPLC. This process was repeated three times ($n = 3$) on the same day using the same sorbent. The intra-assay and inter-assay precision was validated in the same step as above.

Specific recognition of *flavonoids*

As shown in Fig. 1a, the h-BN-MIPs were applied to the selective recognition of the *flavonoids* from *Ginkgo biloba* tea. The pulverized *Ginkgo biloba* tea (5 g) was mixed with methanol (100 mL). In the extraction process, the mixture was treated ultrasonically (20 min) and stirred (8 h) at 50 °C.

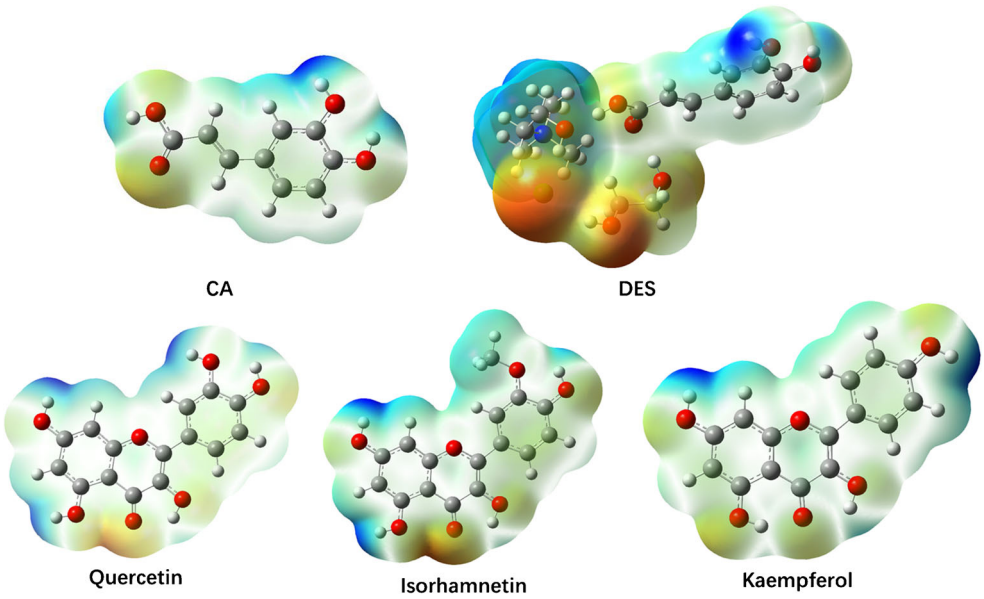

Fig. 2 Electrostatic potential map highlighting the three most susceptible regions to interact via hydrogen bonds with the functional monomers (regions in red)

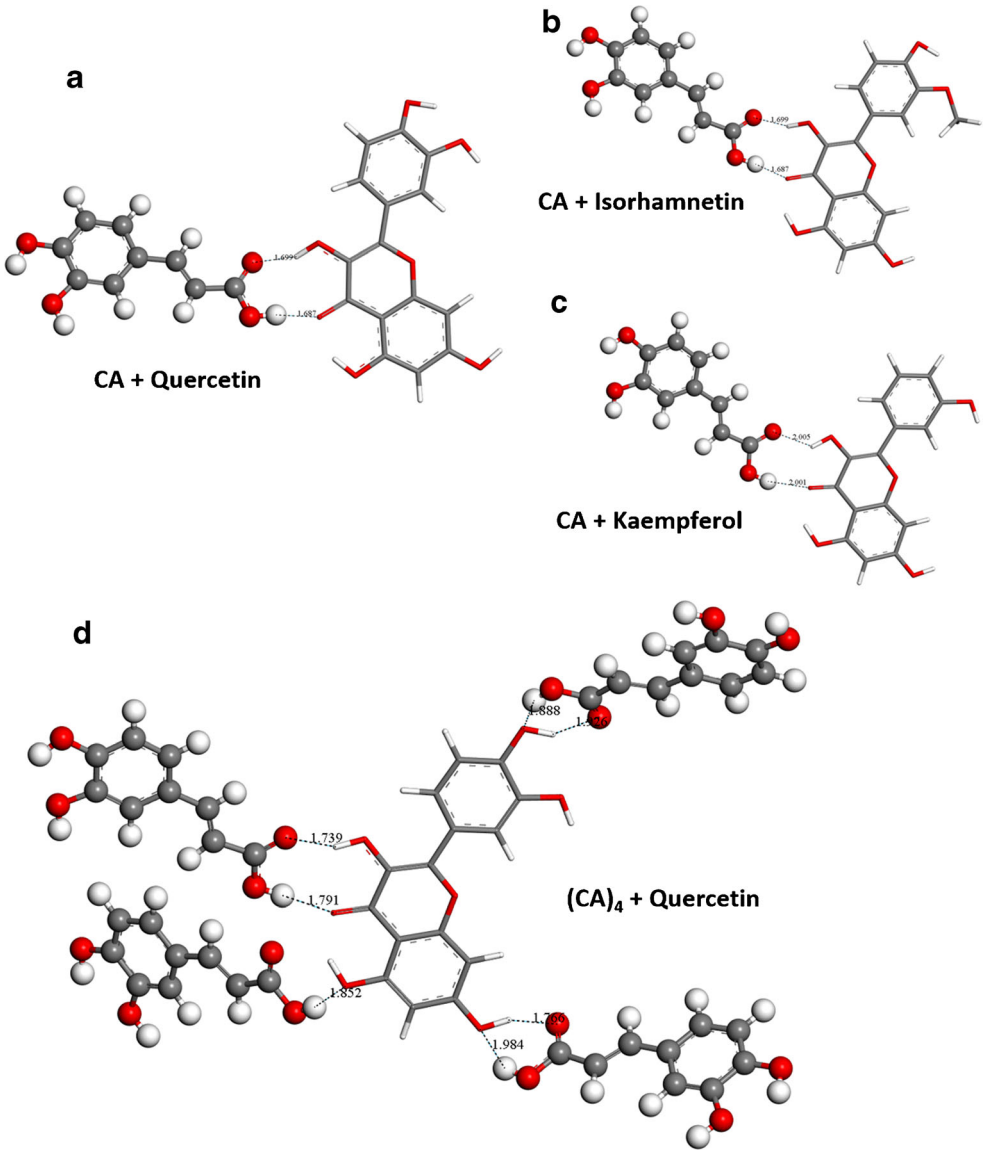

Fig. 3 B3LYP/6-311G+(d,p)-optimized structures for the CA/target complexes. (Hydrogen bonds are drawn in dotted lines for better visualization)

Subsequently, the turbid liquid was left to stand for 1 h and the supernatant was collected. The extract was centrifuged (6000 rpm, 15 min) and filtered before the specific recognition procedure. In the specific recognition (SPE) procedure, the sorbent (200 mg) was packed into an empty SPE column and frits were placed at the lower and upper ends to avoid polymer loss. The extract (1 mL) was added to the SPE column and washed with DI-water (1 mL). After washing, the target was eluted from the SPE column with 1 mL of ethanol. The eluent collected at a constant volume (1 mL) was analyzed by HPLC-UV. This SPE procedure was repeated three times ($n = 3$) using the same SPE column.

Table 1 Thermodynamic properties ΔH, ΔG, ΔE and $T\Delta S$ for complexes. Values are given in kcal mol^{-1}

Complexes	ΔH	ΔG	ΔE	$T\Delta S$	H bonds
CA-Quercetin	−41.16	−0.28	−46.13	−40.88	2
CA-Isorhamnetin	−41.19	−0.32	−46.04	−40.87	2
CA-Kaempferol	−40.79	−0.29	−45.69	−40.5	2
$(CA)_4$-Quercetin	−151.14	−3.42	−172.79	−147.72	7

Results and discussion

Preparation of materials

A type of DESs with different molar ratios were synthesized as the candidate functional monomers. These DESs showed different states at room temperature based on the different intensities of the hydrogen bonds in DESs [17, 28]. DES-4

had the most stable hydrogen bonds (based on the lowest viscosity and highest diaphaneity), and was selected as the optimal functional monomer.

As a common 2D material, h-BN has a large specific surface area. On the other hand, it has strong surface stability and poor dispersion in many solvents. To increase the activated surface groups and enhance the hydrophilicity for h-BN, a surface high temperature oxidation was implemented. After the surface activation treatment, the DES showed excellent dispersibility for processed h-BN. Because of the excellent dispersibility and hydrophilicity of DES, CA (–OH or –COOH) in DES was more likely to interact with the processed h-BN.

EG and ChCl form a DES with CA via hydrogen bonding. To prevent dehydration with a hydroxyl group before polymerization, the –COOH group of CA was protected by the hydrogen bonding of DES. In the preparation of MIPs, the double bond of EGDMA and CA in DES can be cross-linked mutually by thermal-initiated free-radical polymerization in the presence of AIBN. As shown in Fig. 1b, the hydrogen bond of DES was break, CA will break away from the DES and the –COOH group of CA can obtain stable intermolecular hydrogen bonds with the template. In general, based on the special characteristic and abundant hydrogen bond, DES was applied successfully as a novel monomer in the polymerization of h-BN-MIP nanoparticles.

Theoretical studies

BN is an important 2D scaffold material and the structure of the material was examined. Fig. S1c presents the DFT-optimized structure of CA in the DES-modified BN. From this theoretical study, the -OH group of CA was linked to the surface of BN. The choice of high affinity MIP is essential for controlling the interactions between the templates and imprinting molecules. The selection of functional monomers by template interaction analysis allows the choice of a high affinity MIP with control over their binding strength. The chemical structure of DES contains several different heterogeneous interaction sites that can form hydrogen bonds with the target molecules (Que, Iso and Kae) (Fig. S1a). In this sense, an electrostatic potential map (Fig. 2) of the molecular surface of the DES was obtained to determine the possible strong interaction sites. Fig. S1b presents the optimized geometry of the DES and target functional monomers along with their electrostatic map (Fig. 2). The attractive forces between the DES and target molecules in the MIP will occur at the regions colored red (high charge density), as shown in Fig. 2. Based

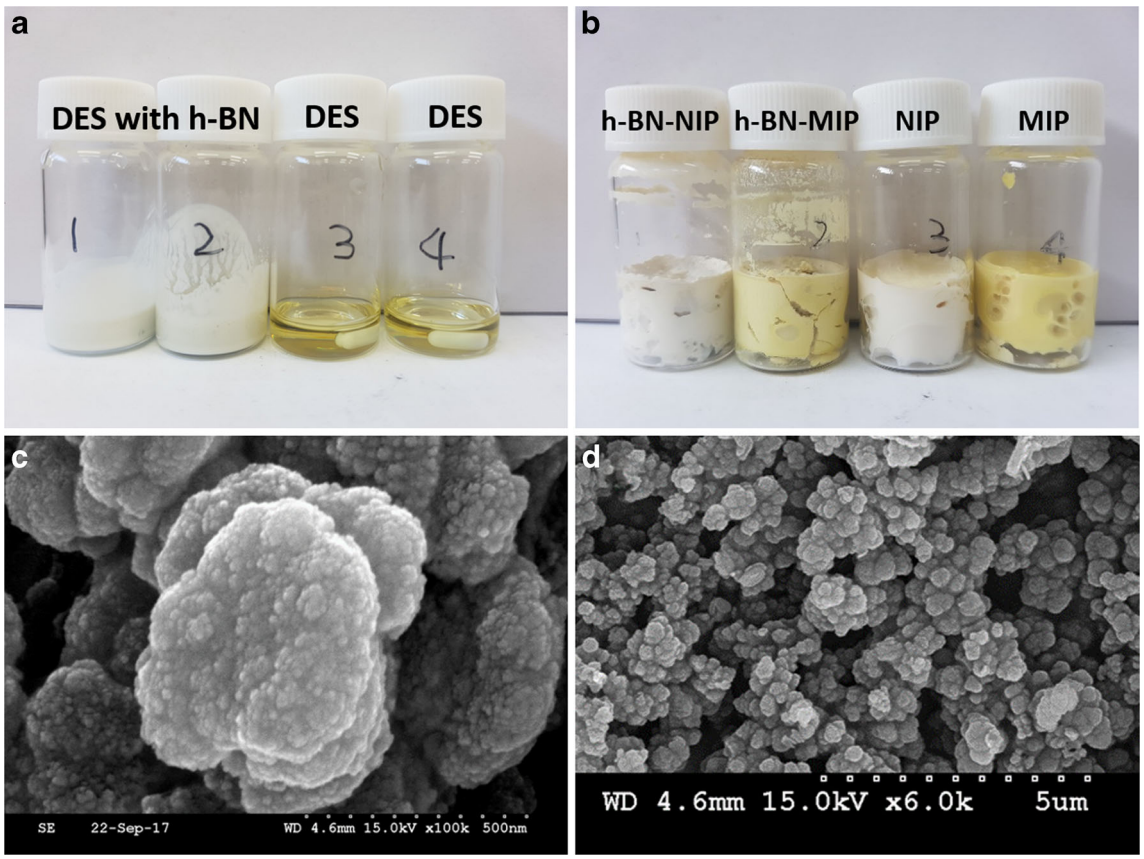

Fig. 4 Image of DES monomer (**a**) and nanoparticles (**b**) before washing. Scanning electron micrograph of h-BN-MIP (**c**) and (**d**)

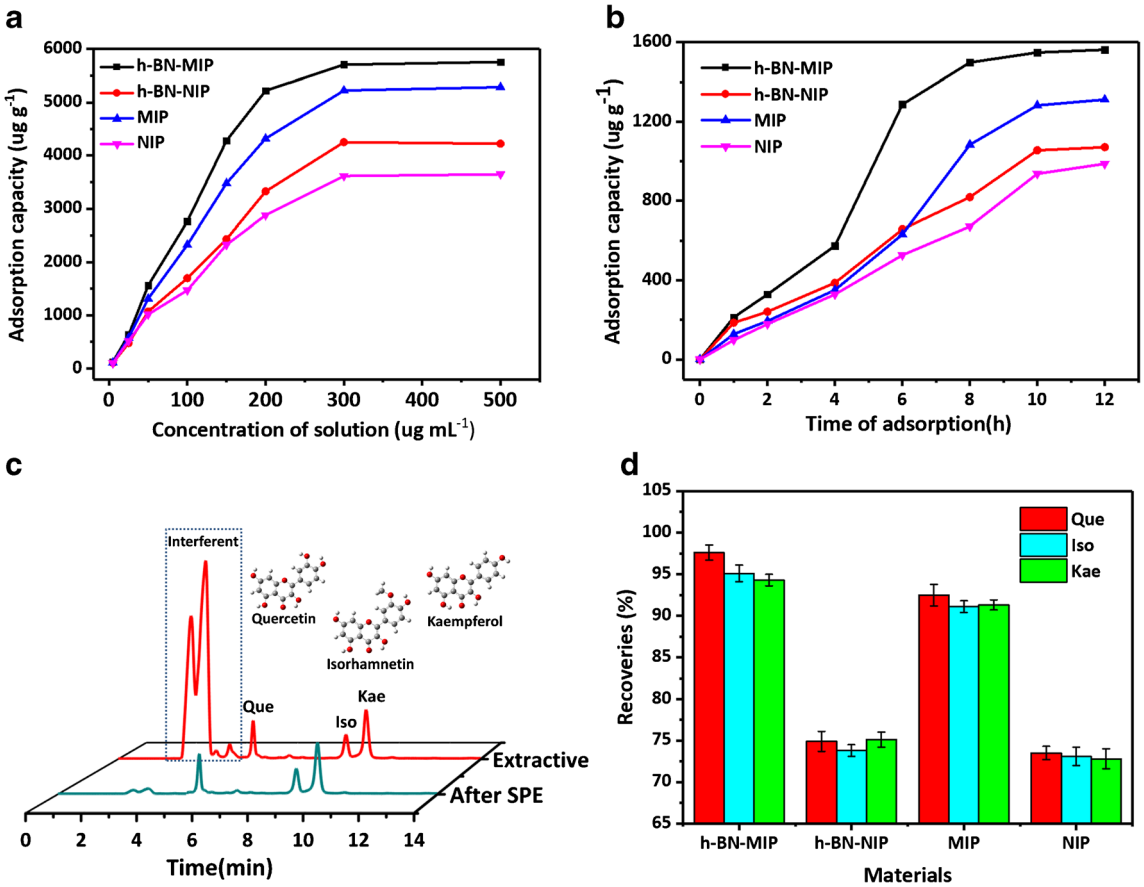

Fig. 5 Static adsorption capacity (**a**) and dynamic adsorption capacity (**b**) of the nanoparticles for quercetin. Chromatogram of *Ginkgo biloba* leaf SPE by h-BN-MIP (**c**). Recovery of flavonoids (**d**)

on the quantitative information from the electrostatic map, the -COOH group of CA can form intermolecular hydrogen bonds with the imprinted molecules (targets) of the regions containing several oxygen sites. In the polymerization of MIP nanoparticles, CA will break away from the DES and polymerize in the MIP nanoparticles.

Figure 3 presents the B3LYP/6-311G(d,p)-optimized structures for the CA-target complexes. As observed in Fig. 3 (a, b and c), all targets (Que, Iso and Kae) can obtain two stable intermolecular hydrogen bonds with CA. Based on the result in Fig. 3d, four CAs can form seven stable intermolecular hydrogen bonds with one Que., and the resulting complex ($(CA)_4$-Que) has a stable structure. On the other hand, the thermodynamic properties (ΔH, ΔG, ΔE, and $T\Delta S$) of the CA–target complexes were calculated, as shown in Table 1. Based on the results in Table 1, CA-target complexes had a very small energy differences (ΔH and ΔG), < 0.5 kcal mol^{-1}. Therefore, the MIPs had similar selectivity for the targets (Que, Iso and Kae). From the above, the design of a MIP based on DES and h-BN is viable. DES can be applied to in the polymerization of h-BN-MIP as an ecofriendly functional monomer.

Table 2 Validation of re-usability recoveries (n = 3) and RSD values of *quercetin* standard solution

Spiked (μg /mL)	Intra-day		Inter-day	
	Recovery (%)	RSD (%)	Recovery (%)	RSD (%)
5	99.8	0.4	100.1	1.0
25	98.9	1.1	99.7	0.7
50	100.3	0.8	99.5	0.9

Characteristics of the materials

As shown in Fig. S2, both h-BN and processed h-BN have a similar 2D structure (disk-shaped) and the structure had a large specific surface area. Nevertheless, the surface roughness of the processed h-BN was increased after surface activation (Fig. S2b). The variation between h-BN and processed h-BN was based on the strong thermostability and surface activation. Based on Fig. 4c–h-BN-MIP was found to be a disk-shaped particle. Although no oblate particles formed, such as thin plates, the polymer adhered to the particle surface (Fig. 4c). The particle sizes of h-BN-MIP (Fig. 4c) were

similar to the h-BN (Fig. S2a), and many polymers wrapped around the surface of the material. From the oblate 2D structure, the h-BN-MIP showed a significantly higher surface area than common MIPs. Therefore, the adsorption capacity and selectivity might benefit substantially from such particle aggregation.

After surface activation, the BET surface area of BN (without exfoliation) was relatively unchanged. As shown in Table S3, h-BN-MIPs (59.35 m^2 g^{-1} and 51.27 m^2 g^{-1}) showed a larger surface area than MIPs (29.81 m^2 g^{-1} and 28.74 m^2 g^{-1}). In this study, the h-BN-MIPs also showed a larger surface area than the MIPs reported in previous studies [9, 28]. The increase in surface area should be based on the introduction of the h-BN scaffold. The nanoparticles synthesized with the template (MIP and h-BN-MIP) had a larger mean pore size and porous volume than the materials synthesized without the template (NIP and h-BN-NIP). The mean pore size and porous volume of the h-BN-MIPs were similar to MIPs. Overall, the introduction of the h-BN scaffold resulted in an increase in surface area for the h-BN-MIPs, the variation of the mean pore size and pore volume was based on the template in polymerization.

Purification of flavonoids

Evaluation of the selective adsorption capacity

The adsorption capacity (dynamic adsorption and static adsorption) of these MIPs was measured using a Que. solution at room temperature. According to Fig. 5a, all materials showed a rapid increase in adsorption before 200 μg mL^{-1}. The increase in adsorption was slower with further increases in concentration until saturation adsorption (300 μg mL^{-1}). h-BN-MIP showed the highest adsorption property. The h-BN-MIPs had a better adsorption property than the MIPs. As shown in Fig. 5b, the adsorption capacity of the MIPs and h-BN-MIPs increased with increasing adsorption time before saturation adsorption. The absorption of h-BN-MIPs showed a faster increase than MIPs. The adsorption of all the materials showed a large increase before 10 h. The adsorption saturation of the nanoparticles required approximately 10–12 h. In these materials, the adsorption capacity of h-BN-MIPs was higher than that of the MIPs, and h-BN-MIP showed the fastest adsorption capacity. This result should be based on the h-BN involved in the polymerization of h-BN-MIPs.

Validation of re-usability

H-BN-MIP showed excellent precision and accuracy under the optimized protocols. As shown in Table 2, the intra-day and inter-day recoveries were 98.9%–100.3%, and 99.5%–100.1%, respectively. On the other hand, the RSD (relative standard deviation) of h-BN-MIP from the intra-day and inter-day determination was less than 1.1% and 1.0%, respectively. From the above, the precision and accuracy of the SPE-HPLC method were confirmed.

Specific recognition of flavonoids

All the materials were applied in the SPE of flavonoids from the *Ginkgo biloba* extract. Both MIPs and h-BN-MIPs can remove the interferent cleanly but the recovery of the flavonoids was different. According to Fig. 5c and d, the MIPs (MIP and h-BN-MIP) had a better recovery and selectivity for flavonoids than the NIPs (NIP and h-BN-NIP). As shown in Table S5, the h-BN-MIP showed the highest selectivity (Que 97.6%, Iso 95.1% and Kae 94.3%) and excellent re-usability (RSD lower than 1.0%) for the flavonoids from the extract and. Interferent are

Table 3 Comparison with other reported methods for recognition of quercetin

Adsorbing materials	Detection Method	Pretreatment method	Natural product	Recoveries (%)	RSD (%)	Reference
Double-template MIPs	HPLC-UV	SPE	Green tea	82.88–88.92	1.23–2.46	[29]
DES-MIPs	HPLC-UV	SPE	Herba artemisiae scopariae	94.23	–	[30]
Three-template MIPs	HPLC-UV	SPE	Herba artemisiae scopariae	80.02	–	[31]
MIP@g-C_3N_4	Fluorescence	MIP-probe	Grape juice, tea juice, black tea, red wine	90.7–94.1	2.1–5.5	[32]
Cu- and S- @SnO_2	UV-Vis	D-μ-SPE	Watercress	90.3–97.28	<6	[33]
MIP@SiO_2	HPLC-UV	SPE	Red wine	99.7–100.4	<5	[34]
MrGO-MIP	Electrochemical	MIP/GO/GC	Grape wine	97.4–101.4	0.52–2.89	[35]
DES-MIPs	HPLC-UV	SPE	*Ginkgo biloba* leaves	92.5	0.9–1.2	This research
DES-h-BN-MIPs	HPLC-UV	SPE	Ginkgo biloba leaves	97.6	0.7–1.0	This research

cleanly removed. By comparison with other methods (Table 3), this method had a higher recovery and lower RSD, it should be profit by the larger amount of effective recognition site was formed under the protected of hydrogen bond of DES. Furthermore, this method was more green and safety than other methods with the introduce of DES monomer. Based on the recognition principle of molecular imprinting technique, the specific recognition should be based on the similar molecular structure (Que, Iso and Kae) with template (Que). Therefore, this mothed bad selectivity for the similar molecular structure with target. The h-BN-MIPs had higher recoveries in the purification of similar natural compounds than traditional MIPs in others studies. The high selectivity of h-BN-MIP was based on the 2D oblate structure obtained during the polymerization of h-BN-MIP nanoparticles.

Conclusions

Following previous research [9, 10], h-BN was devised as a 2D scaffold material in the polymerization of h-BN-MIP nanoparticles, MIP nanoparticles were polymerized using the methodology reported elsewhere as a control group. More than that, the design of h-BN-MIP on the surface of h-BN was validated theoretically using the DFT method. DESs plays a key role in the polymerization process, which should be based on the hydrogen bonding system and the special properties of DESs. The recognition site of the monomer is protected by the hydrogen bond of the DES before the MIP is polymerized. The larger amount of effective recognition site was formed under the protected of hydrogen bond of DES. In addition, the nanoparticles had a 2D oblate structure and a large surface area. From the result of recognition, h-BN-MIP nanoparticles showed good re-usability and recognition ability for the flavonoids from the *Ginkgo biloba* extractive. Furthermore, this method was more green and safety than other methods with the introduce of DES monomer. Based on the superiority of this method, it can be extended to the recognition of a wide range of samples in quantitative analytical applications. Therefore, DESs have a wide range of perspectives in the preparation of various materials. On the other hand, the DFT method was less applicable to the design of MIP and DES research. DFT method confirmed the role of DES in the synthesis process. Therefore, this research method is expected to have extensive applications in theoretical studies aimed at optimizing and exploring DES in synthesis process.

Acknowledgements This study was supported by Basic Science Research Program through the National Research Foundation of Korea (NRF) funded by the Ministry of Education (NRF-2019R1A2C1010032).

Compliance with ethical standards

Conflict of interest There are no conflicts to declare.

References

1. Li Y, Xu W, Zhao X, Huang Y, Kang J, Qi Q, Zhong C (2018) Electrochemical sensors based on molecularly imprinted polymers on Fe3O4/graphene modified by gold nanoparticles for highly selective and sensitive detection of trace ractopamine in water. Analyst 143:5849–5856
2. Deshmukh MA, Shirsat MD, Ramanaviciene A, Ramanavicius A (2018) Composites based on conducting polymers and carbon Nanomaterials for heavy metal ion sensing (review). Crit Rev Anal Chem 48:293–304
3. Li X, Choi J, Ahn WS, Row KH (2018) Preparation and application of porous materials based on deep eutectic solvents. Crit Rev Anal Chem 48:73–85
4. Li X, Row KH (2017) Application of deep eutectic solvents in hybrid molecularly imprinted polymers and mesoporous siliceous material for solid-phase extraction of levofloxacin from green bean extract. Anal Sci 33:611–617
5. Wan Y, Wang M, Fu Q, Wang L, Wang D, Zhang K, Xia Z, Gao D (2018) Novel dual functional monomers based molecularly imprinted polymers for selective extraction of myricetin from herbal medicines. J Chromatogr B 2018(1097–1098):1–9
6. Farooq S, Nie J, Cheng Y, Yan Z, Li J, Asim S, Bacha S, Mushtaq A, Zhang H (2018) Molecularly imprinted polymers' application in pesticide residue detection. Analyst 143:3971–3989
7. Zhong C, Yang B, Jiang X, Li J (2018) Current Progress of Nanomaterials in molecularly imprinted electrochemical sensing. Crit Rev Anal Chem 48:15–32
8. Alizadeh T, Althotmdian M, Ganjali RM (2018) An innovative method for synthesis of imprinted polymer nanomaterial holding thiamine (vitamin B1) selective sites and its application for thiamine determination in food samples. J Chromatogr B 1084:166–174
9. Li X, Row KH (2017) Application of novel ternary deep eutectic solvents as a functional monomer in molecularly imprinted polymers for purification of levofloxacin. J Chromatogr B 1068–1069: 56–63
10. Li X, Dai Y, Row KH (2019) Preparation of two-dimensional magnetic molecularly imprinted polymers based on boron nitride and a deep eutectic solvent for the selective recognition of flavonoids. Analyst 144:1777–1788
11. Liu Y, Wang Y, Dai Q, Zhou Y (2016) Magnetic deep eutectic solvents molecularly imprinted polymers for the selective recognition and separation of protein. Anal Chim Acta 936:168–178
12. Sun G, Liu Y, Ahat H, Shen A, Liang X, Xue X, Luo Y, Yang J, Liu Z, Aisa HA (2017) "Two-dimensional" molecularly imprinted solid-phase extraction coupled with crystallization and high performance liquid chromatography for fast semi-preparative purification of tannins from pomegranate husk extract. J Chromatogr A 1505: 35–42
13. Li X, Row KH (2017) Purification of antibiotics from the millet extract using hybrid molecularly imprinted polymers based on deep eutectic solvents. RSC Adv 7:16997–17004
14. Jin CH, Lin F, Suenaga K, Iijima S (2009) Fabrication of a freestanding boron nitride single layer and its defect assignments. Phys Rev Lett 102:195505
15. Hui F, Fang W, Leong WS, Kpulun T, Wang H, Yang H, Villena MA, Harris G, Kong J, Lanza M (2017) Electrical homogeneity of large-area chemical vapor deposited multilayer hexagonal boron nitride sheets. ACS Appl Mater Interfaces 46:39895–39900
16. Lin J, Yuan X, Li G, Huang Y, Wang W, He X, Yu C, Fang Y, Liu Z, Tang C (2017) Self-assembly of porous boron nitride microfibers into Ultralight multifunctional foams of large sizes. ACS Appl Mater Interfaces 51:44732–44739

17. Weng Q, Wang X, Wang X, Bando Y, Golberg D (2016) Functionalized hexagonal boron nitride nanomaterials: emerging properties and applications. Chem Soc Rev 45:3989–4012
18. Li X, Lee YR, Row KH (2016) Synthesis of mesoporous siliceous materials in choline chloride deep eutectic solvents and the application of these materials to high-performance size exclusion chromatography. Chromatographia 79:375–382
19. Li X, Row KH (2016) Development of deep eutectic solvents applied in extraction and separation. J Sep Sci 39:3505–3520
20. Li X, Row KH (2015) Exploration of mesoporous stationary phases prepared using deep eutectic solvents combining choline chloride with 1,2-butanediol or glycerol for use in size-exclusion chromatography. Chromatographia 78:1321–1325
21. Li X, Row KH (2017) Separation of polysaccharides by SEC utilizing deep eutectic solvent modified mesoporous siliceous materials. Chromatographia 80:1161–1169
22. Zhang Q, Vigier KDO, Royera S, Jérôme F (2012) Deep eutectic solvents: syntheses, properties and applications. Chem Soc Rev 41: 7108–7146
23. Li Z, Su K, Ren J, Yang D, Cheng B, Kim CK, Yao X (2018) Direct catalytic conversion of glucose and cellulose. Green Chem 20:863–872
24. Gu Y, Chen S, Jun R, Jia YA, Chen C, Komarneni S, Yang D, Yao X (2018) Electronic structure tuning in Ni3FeN/r-GO aerogel toward Bifunctional Electrocatalyst for overall water splitting. ACS Nano 12:245–253
25. Silva CF, Borges KB, do Nascimento CS (2018) Rational design of a molecularly imprinted polymer for dinotefuran: theoretical and experimental studies aimed at the development of an efficient adsorbent for microextraction by packed sorbent. Analyst 143:141–149
26. Wang X, Wei F (2017) Kinetic study of application of Graphene oxide as a catalyst to accelerate extraction of total flavonoids from Radix Scutellaria. RSC Adv 7:46894–46899
27. Motta EVD, Costa JD, Bastos JK (2017) A validated HPLC-UV method for the analysis of galloylquinic acid derivatives and flavonoids in Copaifera langsdorffii leaves. J Chromatogr B 1061:240–247
28. Fu N, Li L, Liu X, Fu N, Zhang C, Hu L, Li D, Tang B, Zhu T (2017) Specific recognition of polyphenols by molecularly imprinted polymers based on a ternary deep eutectic solvent. J Chromatogr A 1530:23–34
29. Qu Q, Zhu T (2017) Preparation of hybrid-monomer, double-template molecularly imprinted polymers for the purification of green tea extracts. Anal Methods 9:6525–6533
30. Ma W, Tang B, Row KH (2017) Exploration of a ternary deep eutectic solvent of methyltriphenylphosphonium bromide/chalcone/formic acid for the selective recognition of rutin and quercetin in Herba Artemisiae Scopariae. J Sep Sci 40:3248–3256
31. Li G, Ahn WS, Row KH (2016) Hybrid molecularly imprinted polymers modified by deep eutectic solvents and ionic liquids with three templates for the rapid simultaneous purification of rutin, scoparone, and quercetin from Herba Artemisiae Scopariae. J Sep Sci 39:4465–4473
32. Xu S, Chen L, Ma L (2018) Fluorometric determination of quercetin by using graphitic carbon nitride nanoparticles modified with a molecularly imprinted polymer. Microchim Acta 185:492
33. Asfarama A, Ghaedib M, Javadianc H, Goudarzi A (2018) Cu- and S- @SnO2 nanoparticles loaded on activated carbon for efficient ultrasound assisted dispersive μSPE-spectrophotometric detection of quercetin in Nasturtium officinale extract and fruit juice samples: CCD-RSM design. Ultrason Sonochem 47:1–9
34. Zengin A, Badak MU, Aktas N (2018) Selective separation and determination of quercetin from red wine by molecularly imprinted nanoparticles coupled with HPLC and ultraviolet detection. J Sep Sci 41:3459–3466
35. Yao Z, Yang X, Liu X, Yang Y, Hu Y, Zhao Z (2018) Electrochemical quercetin sensor based on a nanocomposite consisting of magnetized reduced graphene oxide, silver nanoparticles and a molecularly imprinted polymer on a screen-printed electrode. Microchim Acta 185:70